ISSN 0023-1584, Kinetics and Catalysis, 2020, Vol. 61, No. 4, pp. 623–630. © Pleiades Publishing, Ltd., 2020.

Mechanistic Studies of Methanol Synthesis Reaction over Cu and Pd–Cu Catalysts

**R. Ciesielski[a, *], O. Shtyka[a], M. Zakrzewski[a], J. Kubicki[a], W. Maniukiewicz[a],
A. Kedziora[a], and T. P. Maniecki[a]**

[a] *Lodz University of Technology, Lodz, 90-924 Poland*

**e-mail: radoslaw.ciesielski@p.lodz.pl*

Received December 6, 2019; revised January 10, 2020; accepted January 21, 2020

Abstract—Monometallic copper and bimetallic palladium–copper catalysts supported on $ZnO–Al_2O_3$, $CeO_2–Al_2O_3$ and $ZrO_2–Al_2O_3$ were prepared by conventional impregnation method and tested in the methanol synthesis reaction in a gradient less reactor under elevated pressure (3.5 MPa) at 220°C. The physicochemical properties of prepared catalytic systems were studied using BET, TPR-H_2, TPD-NH_3, XRD, SEM-EDS and FT-IR techniques. The results of XRD and SEM-EDS measurements showed the formation of Pd–Cu alloy during the activation of bimetallic catalysts. It was found that the formed alloy was responsible for the improved activity and selectivity of catalysts in the studied reaction. Among investigated catalysts, the highest formation rate of methanol was observed with 2%Pd–20%Cu/$ZnO–Al_2O_3$ system. Based on the results of FT-IR measurements it can be concluded that hydrogen molecules adsorb dissociatively on the metallic copper surface to form hydrogen atoms, increasing the hydrogen spillover effect on the metal-support interface. In contrast, CO_2 adsorb on the oxygen vacancies of the support to form carbonates, which can further undergo hydrogenation to methanol.

Keywords: methanol synthesis, CO_2 hydrogenation, palladium-copper catalysts, Pd–Cu alloy, binary oxide, reactive intermediates

DOI: 10.1134/S0023158420040035

INTRODUCTION

The atmospheric concentrations of CO_2 have been increasing steadily for last decades. The combustion of fossil fuels is the largest contributor to the CO_2 emission [1]. Without proper emission management, this could lead to significant climate changes. Therefore, the effective utilization of CO_2 and mitigating the fossil fuel dependence are of prime interest of the scientific community [1–4].

Methanol (CH_3OH) is an important chemical feedstock, as well as an energy storage medium [5]. The production of CH_3OH from CO_2 involves the exothermic CO_2 hydrogenation (Eq. (1)) and endothermic reverse water gas shift reaction (RWGS, Eq. (2))

$$CO_2 + 3H_2 = CH_3OH + H_2O, \quad \Delta H_{298\,K} = 49.4\ \text{kJ/mol}, \tag{1}$$

$$CO_2 + H_2 = CO + H_2O, \quad \Delta H_{298\,K} = 41.0\ \text{kJ/mol}. \tag{2}$$

Thermodynamically, CO_2 hydrogenation to CH_3OH is less favorable than hydrogenation of CO [6]. At 523 K and 4.0 MPa, the CH_3OH yield at equilibrium via CO_2/H_2 is 14%, while equilibrium yield through CO/H_2 is as high as 50% [7]. Such a striking difference makes the route to convert CO_2 into methanol more challenging than syngas conversion. Over the past decades, significant efforts have been directed to developing Cu–Zn-based catalysts for CH_3OH synthesis from both syngas conversion and CO_2 hydrogenation [9, 10]. On the other hand, palladium systems gained attention as catalysts for CO_2 hydrogenation due to their high activity in CO_2 hydrogenation to methanol in comparison with Cu–ZnO based catalysts [11, 12]. Numerous data confirmed that supported Pd nanoparticles are actually active in the synthesis of CH_3OH from H_2/CO_2 [13–17].

The main goal of this study was to investigate the physicochemical and catalytic properties of the copper (10, 20 and 40 wt % of Cu) and palladium–copper

---

Abbreviations: RWGS, reverse water gas shift reaction; TPR-H_2, H_2 temperature-programmed reduction; TCD, a thermal conductivity detector; TPD-NH_3, NH_3 temperature programmed desorption; SEM, scanning electron microscopy; EDS – energy dispersive X-ray spectroscopy; GC, gas chromatography; XRD, X-ray diffraction; FT-IR, Fourier-transform infrared spectroscopy.

(2 wt % of Pd and 20 wt % of Cu) catalysts supported on ZnO–Al_2O_3, ZrO_2–Al_2O_3, CeO_2–Al_2O_3 binary oxides Their activity in the reaction of methanol synthesis from a CO_2/H_2 mixture was evaluated. Compared to monoxide supports such systems are characterized by a well-developed specific surface and improved stability [18]. By a proper selection of both the qualitative and quantitative composition of the support it is possible to control its physicochemical properties such as specific surface, acid–base nature of the surface, and susceptibility to reduction. The composition of the support and the active phase has a significant impact on mechanical and thermal resistance, carbon deposition tolerance, specific surface area and hydrophobicity of the catalyst. Such parameters shape the properties of the supported catalyst, primarily its selectivity and activity in the studied catalytic process.

EXPERIMENTAL

Copper and palladium-copper catalysts were prepared by wet aqueous impregnation. In order to prepare ZnO–Al_2O_3, CeO_2–Al_2O_3 and ZrO_2–Al_2O_3 supports with the targeted molar ratio of Zn : Al, Ce : Al and Zr : Al = 0.5, nitrates of zinc, cerium, zirconium and aluminum were used. Aqueous solutions of 1 mol/dm^3 zinc/cerium/zirconium nitrate and 1 mol/dm^3 aluminum nitrate were mixed in appropriate quantity under vigorous stirring at 80°C. A concentrated ammonia solution was then added dropwise to the solution until the solution pH reached values between 10 and 11 and then the mixtures were stirred for another 30 min. The resulting fine precipitates were washed two times with deionised water and then dried at 120°C for 15 h and calcined for 4 h at 400°C in air. Metal phase Cu and Pd was introduced on the previously prepared supports surface by wet impregnation using aqueous solutions of copper and palladium nitrates. The supported catalysts were then dried in air at 120°C for 2 h and finally calcined for 4 h in air at 400°C. Copper and palladium loadings were 10–40 and 2 wt %, respectively.

The specific surface areas of supports and catalysts were determined by nitrogen adsorption (77 K) employing the BET method with an automatic Sorptomatic 1900 apparatus.

The temperature-programmed reduction (TPR-H_2) measurements were carried out in an automatic TPR system AMI-1 in the temperature range of 25–900°C with a linear heating rate of 10°C/min. Transfer line between reactor and detector was heated up to 120°C. Before analysis, the samples were heated in an argon stream at 400°C for 2 h to remove water and impurities from catalytic systems. Samples (about 0.1 g) were reduced in hydrogen stream (5% H_2–95% Ar) with a volumetric flow rate of 40 cm^3/min. Hydrogen consumption was monitored by a thermal conductivity detector (TCD).

The procedure used to characterize the catalyst surface acidity includes the purification of catalyst surface, adsorption of ammonia and NH_3 temperature programmed desorption (TPD-NH_3). The method applied to purify the catalyst could lead to dihydroxylation of the catalyst surface. The sample (about 0.15 g) was flushed with pure argon stream (40 cm^3/min, 400°C, 2 h) to remove water from the system. After cooling the sample to 50°C in argon, a gaseous ammonia flow (0.5 h) was introduced into the sample tube to entirely saturate the catalyst surface. After NH_3 adsorption, the excessive amount of weakly and physically adsorbed ammonia on the catalyst surface was removed by flushing the catalyst in pure argon stream with (40 cm^3/min). TPD-NH_3 measurements were made in a temperature range of 100–600°C with a linear heating rate of 25°C/min using TCD detector.

The diffraction patterns were recorded using CuK_α radiation on a PANalytical X'Pert Pro diffractometer in the 2θ range from 5° to 90° with steps of 0.167° and $\Delta t = 10$ s. Since the initial diffraction data may contain interference, the background during the analysis was recorded using the Sonneveld–Visser algorithm [19]. All the calculations were carried out using the X'PertHighScore Plus computer program.

The SEM measurements were made by scanning electron microscopy (SEM) and energy dispersive X-ray spectroscopy (EDS), respectively, on the equipment JSM-6010PLUS/LA (JEOL). The EDS method made it possible to qualitatively determine elements present in the studied micro-area of the sample surface layer on the basis of the obtained characteristic X-ray spectra. A map of the distribution of elements on the studied micro-area was made. The accelerating voltage was 20 kV. For the analysis, the samples were coated with a carbon target using a Cressington 208 HR system.

The IR spectra were taken on a Shimadzu IRTracer-100 equipped with a mercury cadmium telluride detector. Prior to the analysis, the catalysts were reduced in situ at 300°C in an atmosphere of 5% H_2 and 95% argon for 2 h. After reduction, the samples were cooled to 220°C and the gas stream was switched over to the reaction mixture of H_2 and CO_2 (3 : 1 mole ratio).

Activity tests in methanol synthesis reaction were carried out in the gradient less reactor using a gas mixture of H_2 and CO_2 with a molar ratio of 3 : 1. The total flow rate of the reaction mixture was 80 cm^3/min. Process was carried out under pressure (3.5 MPa) at

220°C and products were analyzed by gas chromatography (GC). The accuracy of the chromatographic measurements was at a precision level of 5%. The temperature was measured using Class A thermoelectric elements, placed directly in the catalyst bed, which ensures accuracy of 1°C of the range of measured temperatures. Before activity tests all catalysts were prereduced for 2 h in a flow of 5% H_2–95% Ar mixture at 300°C under atmospheric pressure. The steady-state activity measurements were taken after at least 12 h on the stream. The analysis of the gaseous reaction products were carried out by an on-line GC equipped with a flame ionization detector (FID) and 10% Carbowax 1500 on Graphpac column. The transfer line from the outlet of the reactor to the GC was heated to 120°C to prevent condensation of reaction products. The CO and CO_2 concentrations were monitored by GC chromatograph equipped with TCD detector (120°C, 130 mA) and Carbosphere 60/80 (65°C) column. The catalytic activity of the investigated systems was expressed as the amount of product formed on the mass of catalyst per unit of time (g_{CH_3OH} kg_{cat}^{-1} h^{-1}).

RESULTS AND DISCUSSION

Table 1 contains the results of activity tests in methanol synthesis carried out by converting CO_2 and H_2over copper and bimetallic palladium–copper catalysts supported on binary oxides ZnO–Al_2O_3, ZrO_2–Al_2O_3, CeO_2–Al_2O_3.

As can be seen from the obtained results, the main reaction products were methanol, carbon monoxide and small amounts of methane. Additionally, the formation of trace amounts of dimethyl ether and formaldehyde was also observed. It is worth mentioning that no byproducts were formed when the process was performed without catalyst. Also, the activity measurement showed that an increase in copper content leads to deterioration of the catalytic activity of copper systems regardless of the support used. The similar results were obtained by Ahouari et al. [20]. They investigated the effect of copper concentration on the activity of CuO–ZnO–Al_2O_3 catalyst in the reaction of methanol synthesis (250°C at 3.0 MPa). It was found that the catalyst with the copper load of 51% was the most active while the further increase in Cu concentration (up to 72%) resulted in decreasing rate of

Table 1. The activity results for methanol synthesis from a mixture of H_2 and CO_2 over copper and palladium-copper catalysts supported on binary oxides ZnO–Al_2O_3, ZrO_2–Al_2O_3 and CeO_2–Al_2O_3

Catalyst	Selectivity, %					MeOH yield, g_{CH3OH} g_{CH_3OH} $kg_{cat}^{-1}h^{-1}$
	CO	CH_3OH	CH_4	CH_3OCH_3	HCHO	
Empty reactor	0.00	100	0.00	0.00	0.00	19
10%Cu/CeO_2–Al_2O_3	30.42	66.75	2.80	0.02	0.01	430
20%Cu/CeO_2–Al_2O_3	21.74	76.28	1.95	0.02	0.01	325
40%Cu/CeO_2–Al_2O_3	0.00	94.80	5.17	0.02	0.01	280
2%Pd–20%Cu/CeO_2–Al_2O_3	1.13	98.77	0.00	0.08	0.02	336
10%Cu/ZnO–Al_2O_3	28.55	70.85	0.50	0.07	0.03	681
20%Cu/ZnO–Al_2O_3	25.83	73.21	0.92	0.03	0.01	636
40%Cu/ZnO–Al_2O_3	4.04	94.96	0.93	0.05	0.02	619
2%Pd–20%Cu/ZnO–Al_2O_3	1.15	98.20	0.61	0.03	0.01	715
10%Cu/ZrO_2–Al_2O_3	21.52	78.46	0.00	0.02	0.00	687
20%Cu/ZrO_2–Al_2O_3	20.07	79.90	0.00	0.02	0.01	637
40%Cu/ZrO_2–Al_2O_3	14.37	84.90	0.70	0.02	0.01	640
2%Pd–20%Cu/ZrO_2–Al_2O_3	9.30	90.08	0.58	0.02	0.02	667

Reaction conditions: H_2/CO_2 ratio in the feed = 3, temperature = 220°C, total pressure = 3.5 MPa, weight of catalyst = 0.2 g, total flow of the reaction mixture = 80 cm^3/min.

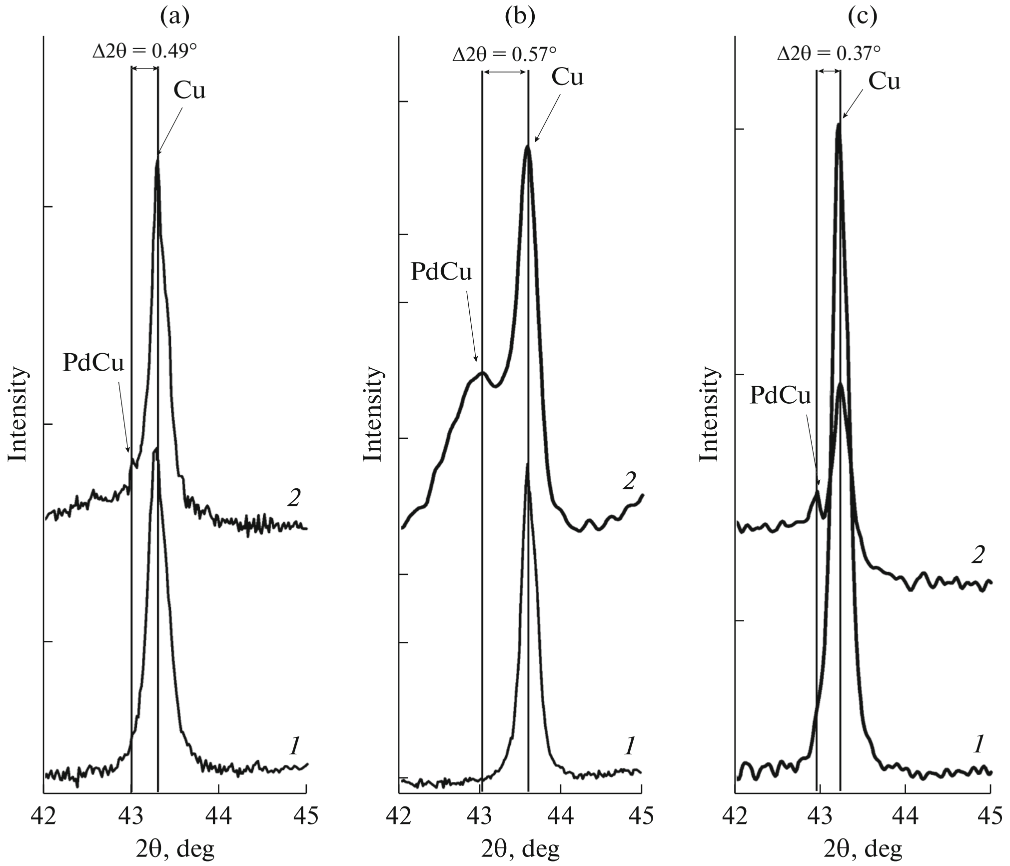

Fig. 1. XRD profiles of Cu (*1*) and Pd–Cu (*2*) catalysts supported on CeO_2–Al_2O_3 (a), ZnO–Al_2O_3 (b) and ZrO_2–Al_2O_3 (c) after reduction at 300°C for 2 h.

methanol formation. The authors noted that the catalytic activity increased with an increase in the surface area of metallic copper, but a linear relationship was not observed. From this result a suggestion was made that the size of copper metallic surface and the specific interaction between copper and support are the main factors that affect the catalytic activity. Based on the results presented in Table 1, it is easily to conclude that the increase in the Cu content in the tested catalytic system leads to increasing selectivity towards the main product – methanol. Also, it can be seen, that the addition of palladium to monometallic copper catalysts resulted in enhanced formation of methanol. Such effect can be attributed to the formation of an alloy Pd–Cu during the activation process in hydrogen mixture as evidenced by X-ray diffraction (XRD) patterns (Fig. 1).

In order to confirm this assumption, the physicochemical measurements of the investigated catalysts were performed (Table 2). From these results, it can be inferred that the activity of catalysts is closely related to their susceptibility to the reduction. The TPR profile acquired from the measurements performed for Cu/ZrO_2–Al_2O_3 showed the presence of two peaks (T_2 and T_3 in Table 2, Fig. 2) attributable to the reduction of copper(II) and copper(I) oxides, respectively. The same peaks associated with the reduction of copper were observed for Cu/ZnO–Al_2O_3 systems. A high-temperature shift of the maxima of the second reduction peak with increasing Cu content also merits consideration. In contrast, the TPR profile of Cu/CeO_2–Al_2O_3 showed three reduction peaks (Fig. 2a). The first two peaks were due to the reduction of highly dispersed CuO and copper ions interacting with the support (T_2, T_3), respectively. The last peak of hydrogen uptake (about 850°C) was attributed to the reduction of large clusters of CuO in the bulk of the support. Similarly, as in the previous case, a shift of the reduction peak towards higher temperatures with increasing copper content was observed. It is worth emphasizing that the catalysts least susceptible to the reduction were also characterized by the lowest activity in the investigated reaction (Tables 1 and 2).

The similar TPR results were observed by Zhang et al. [21] and Huang et al. [22]. They investigated the reducibility of copper catalysts (5–70 wt %) supported

Table 2. Activity results and physicochemical properties of supported mono- and bimetallic catalysts

Catalyst	MeOH yield, $g_{CH3OH}\ kg_{cat}^{-1}\ h^{-1}$	TPR (temperature of the maximum reduction rate)			Total acidity of the surface, $mmol/g_{cat}$	Specific surface area, m^2/g
		T_1, °C	T_2, °C	T_3, °C		
$CeO_2–Al_2O_3$	–	–	380	–	0.59	144
10%$Cu/CeO_2–Al_2O_3$	430	–	201–213	265	0.64	111
20%$Cu/CeO_2–Al_2O_3$	325	–	200–216	295	0.45	128
40%$Cu/CeO_2–Al_2O_3$	280	–	202–213	330	0.31	63
2%Pd–20%$Cu/CeO_2–Al_2O_3$	336	130	180	240	0.44	116
$ZnO–Al_2O_3$	–	–	–	–	0.99	251
10%$Cu/ZnO–Al_2O_3$	681	–	203	248	0.98	191
20%$Cu/ZnO–Al_2O_3$	636	–	206	271	0.78	185
40%$Cu/ZnO–Al_2O_3$	619	–	203–250	296	0.57	113
2%Pd–20%$Cu/ZnO–Al_2O_3$	715	105	141	193	0.86	172
$ZrO_2–Al_2O_3$	–	–	–	–	1.65	252
10%$Cu/ZrO_2–Al_2O_3$	687	–	214	251	0.85	160
20%$Cu/ZrO_2–Al_2O_3$	637	–	215	266	0.66	164
40%$Cu/ZrO_2–Al_2O_3$	640	–	214	320	0.42	105
2%Pd–20%$Cu/ZrO_2–Al_2O_3$	667	120	187	233	0.73	159

on SiO_2 and ZnO/ZrO_2. It was reported that increasing in the metal load results in an increase in the reduction temperature of catalysts.

The TPR profiles of catalysts promoted by palladium exhibited additional reduction peak (T_1 in Table 2) in the low temperature range of 105–130°C, which can be attributed to the reduction of palladium oxide particles. A low-temperature shift of maxima of reduction peak of copper oxide species compared with those of unpromoted catalysts is worth noting. This indicates that the addition of Pd into the copper catalyst facilitates the reduction of copper oxide species by the spillover effect developed between Pd and CuO [23, 24]. The reducibility of catalysts strongly correlates with the activity in the studied reaction. For instance, the catalyst 2%Pd–20%$Cu/ZnO–Al_2O_3$ with the easiest reducibility was characterized by the highest formation rate of methanol.

The results of reducibility measurements were in a good correlation with those obtained by XRD tech-

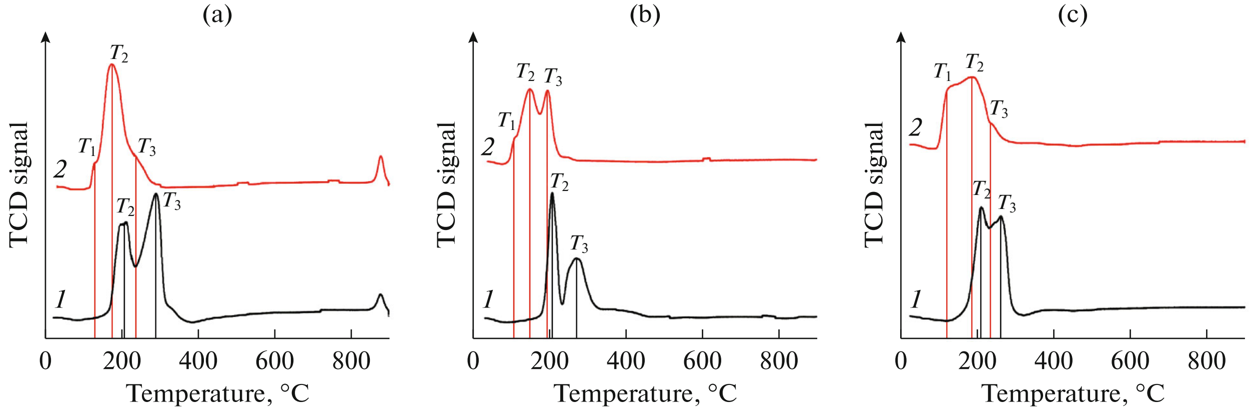

Fig. 2. TPR profiles of Cu (*1*) and Pd–Cu (*2*) catalysts supported on $CeO_2–Al_2O_3$ (a), $ZnO–Al_2O_3$ (b) and $ZrO_2–Al_2O_3$ (c) after calcination in air atmosphere at 400°C for 4 h.

Table 3. Surface characteristics of mono- and bimetallic catalysts

Catalyst	Pd/Cu atomic ratio on the catalyst surface*	Amount on the surface, at %*		Amount in the active phase, at %**		Crystallite size, nm**	
		Pd	Cu	PdCu	Cu	Cu	PdCu
20%Cu/CeO_2–Al_2O_3	–	–	14.78	–	–	71	–
2%Pd–20%Cu/CeO_2–Al_2O_3	0.03	0.90	29.90	12.6	86.4	68	6
20%Cu/ZnO–Al_2O_3	–	–	14.61	–	–	74	–
2%Pd–20%Cu/ZnO–Al_2O_3	0.50	12.22	24.08	42.8	57.2	52	10
20%Cu/ZrO_2–Al_2O_3	–	–	19.59	–	–	87	–
2%Pd–20%Cu/ZrO_2–Al_2O_3	0.05	0.94	18.57	28.6	71.4	62	5

* Determined by EDS measurements, after reduction in a mixture of 5%H_2–95%Ar at 300°C.
** Calculated based on XRD measurements, after reduction in a mixture of 5%H_2–95%Ar at 300°C.

nique. It was found that catalysts with the smallest size of copper particles underwent reduction readily while the samples with the biggest particle size were the least susceptible to the reduction (Tables 2 and 3). The order of decreasing reducibility for the investigated catalysts was found to be: 2%Pd–20%Cu/ZnO–Al_2O_3 (the average size of Cu particles was 52 nm) > 2%Pd–20%Cu/ZrO_2–Al_2O_3 (62 nm) > 2%Pd–20%Cu/CeO_2–Al_2O_3 (68 nm).

The acidity measurements carried out for mono- and bimetallic catalysts showed that the deposition of copper oxide onto the surface of supports bring about a decrease in their total acidity. The opposite effect was observed when palladium was added into the copper catalyst. It is worth noting that the highest total amount of desorbed NH_3 was observed for 2%Pd–20%Cu/(ZnO–Al_2O_3) catalyst (0.86 mmol NH_3/g_{cat}). The differences in the surface acidity of mono- and bimetallic catalysts also correlate with their activity in the investigated reaction. It can be suggested that the catalysts with the highest acidity stronger stabilize the intermediates formed during the methanol synthesis and in this way improve the catalytic activity.

The surface content of active metals was estimated by means of SEM-EDS measurements (Table 3). The obtained results suggested that the distribution of metal particles deposited on the surface of supports was not homogeneous, as evidenced by large differences in the atomic percentage of individual metals. Interestingly, 2%Pd–20%Cu/CeO_2–Al_2O_3 catalyst which had the lowest Pd/Cu ratio was also the least active among the bimetallic catalysts. Moreover, this sample had the lowest relative concentration of Pd–Cu alloy and the largest size of copper particles. On the other hand, the 2%Pd–20%Cu/ZnO–Al_2O_3 catalyst, which was proved to be the most active system, was characterized by the highest surface Pd/Cu ratio (0.50), highest relative concentration of Pd–Cu alloy (42.8%), and, at the same time, by the smallest size of copper crystallites. The similar results were also obtained by other investigators. Jiang et al. [25, 26] reported that the atomic ratio of Pd and Cu has a crucial influence on the course of hydrogenation of CO_2 to CH_3OH. Hu et al. [27] investigated the activity of PdCu–ZnO catalysts (with different Pd loading) in the same process. The authors observed the same relationship between the methanol yield and the Pd/Cu ratio in the catalytic system. It was reported that the most active catalyst produced a system containing 1% Pd (Pd/Cu = 0.01) since the yield of methanol was 2.5 times that reported for the non-promoted Cu–ZnO catalyst. Such observation can be explained by enhanced interactions between Pd and Cu that intensify the hydrogen spillover effect during the hydrogenation of CO_2 to methanol. Also, the formation of Pd–Cu alloy modifies the redox properties of the Cu surface, preventing the oxidation of copper metal by CO_2 during the process [28].

In order to investigate the reaction mechanism, in situ Fourier-transform infrared spectroscopy (FT-IR) measurements were performed to identify intermediate species formed on the surface of both catalysts and supports during the reaction (Fig. 3).

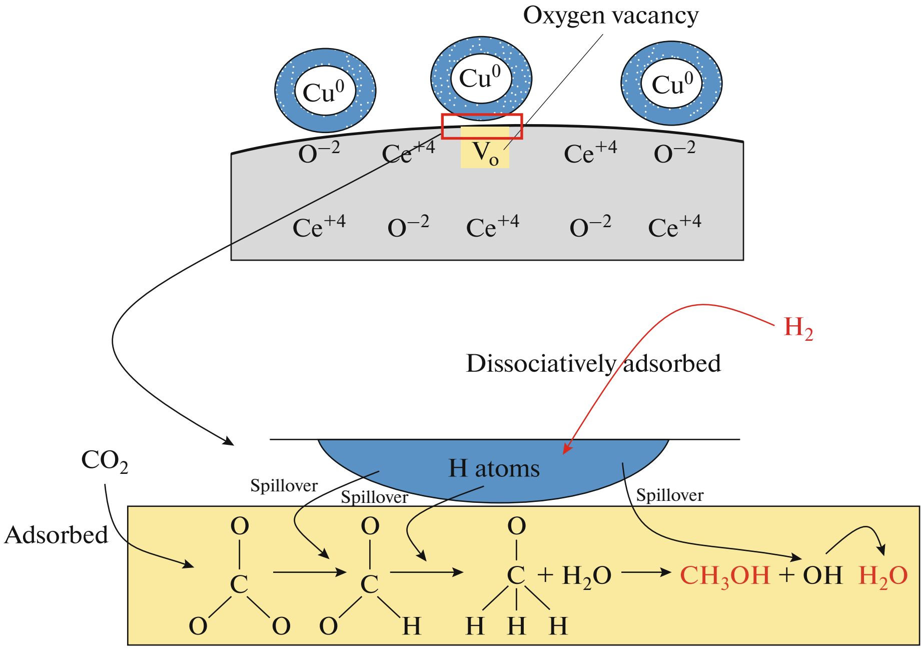

Scheme 1. Scheme of proposed mechanism for CO_2 hydrogenation to methanol.

The IR spectra of CeO_2 showed adsorption bands attributable to cerium formates (b-HCO_2-Ce: 1335, 1520 and 2958 cm^{-1} and m-HCO_2-Ce: 2867 cm^{-1}), as well as methoxy groups (1065, 2824 cm^{-1}). The spectrum obtained for CeO_2–Al_2O_3 showed additional absorption bands at 1570 and 2856 cm^{-1} associated with the corresponding formate species (b-HCO_2-Al). Furthermore, the addition of copper led to the appear-

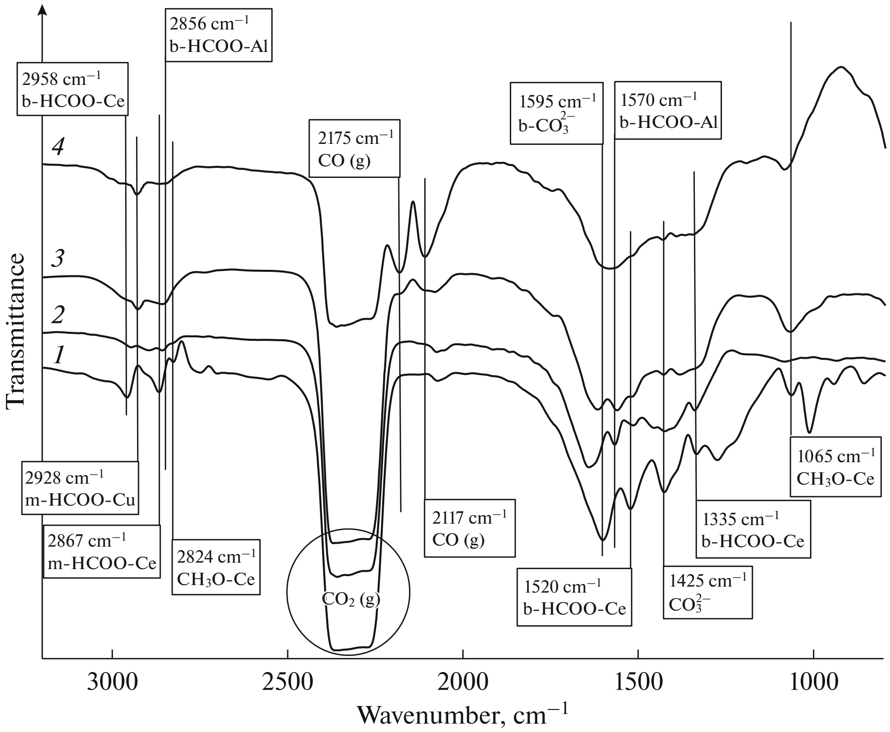

Fig. 3. IR spectra of adsorbed forms of the intermediates formed in the synthesis of methanol from a mixture of H_2 and CO_2 at 220°C on the systems: CeO_2 (*1*), CeO_2–Al_2O_3 (*2*), 20%Cu/CeO_2–Al_2O_3 (*3*), 2%Pd–20%Cu/CeO_2–Al_2O_3 (*4*).

ance of a band at 2928 cm^{-1} corresponding to the b-HCO_2-Cu group. Besides, an increase in the intensity of methoxy CH_3O–Ce band located at 1065 cm^{-1} was observed, indicating a synergetic interaction between the support and the active metal phase. In the case of palladium-copper catalyst, the additional bands were identified at 2117 and 2175 cm^{-1}. These bands were due to the presence of gaseous CO, which was formed because of CO_2 dissociation through the RWGS reaction.

Base on the IR measurement results as well as literature review, a reaction mechanism of methanol synthesis reaction was proposed (Scheme 1).

The reaction starts with the adsorption of both hydrogen and CO_2 molecules. The hydrogen adsorbs dissociatively on the copper metal surface to form hydrogen atoms, which then migrate to the metal-support interface. At the same time, gaseous CO_2 adsorbs on oxygen support vacancies to form carbonates. Next, the adjacent hydrogen atoms interact with the carbonate groups, forming intermediate formate species. The formed groups are further hydrogenated to methoxy species and water. In the next step, the methoxy intermediates react with the formed water to yield methanol and hydroxyl groups. In the final step, the hydroxyls are hydrogenated by atomic hydrogen to form water.

CONCLUSIONS

This work confirms the promotion effect of palladium on the activity and selectivity of copper catalysts in the methanol synthesis reaction. The improvement in the activity of bimetallic catalysts was explained by the formation of Pd–Cu alloy. Additionally, the presence of supported palladium atoms promotes the activation of hydrogen due to the spillover effect, as evidenced by the low-temperature shifts of reduction temperatures of catalysts towards. The obtained results also revealed that the increase in copper content was accompanied by simultaneous decrease in the total acidity and specific surface area of the investigated catalysts. This leads to the low catalytic activity of the catalysts. FT-IR in situ studies of CO_2 hydrogenation showed the occurrence of HCO^{2-} and CH_3O^- species on the surface of the support. The presence of these forms implies that CO_2 is adsorbed on the surface of the support and then is hydrogenated to intermediate surface species in subsequent reaction steps.

REFERENCES

1. Davis, S.J., Caldeira, K., and Matthews, H.D., *Science*, 2010, vol. 329, no. 5997, p. 1330.
2. Pontzen, F., Liebner, W., Gronemann, V., Rothaemel, M., and Ahlers, B., *Catal. Today*, 2011, vol. 171, no. 1, p. 242.
3. Ansari, M.B., and Park, S.-E., *Energy Environ. Sci.*, 2012, vol. 5, no. 11, p. 9419.
4. Raudaskoski, R., Turpeinen, E., Lenkkeri, R., Pongrácz, E., and Keiski, R.L., *Catal. Today*, 2009, vol. 144, no. 3, p. 318.
5. Räuchle, K., Plass, L., Wernicke, H.-J., and Bertau, M., *Energy Technol.*, 2016, vol. 4, no. 1, p. 193.
6. Inui, T., Hara, H., Takeguchi, T., and Kim, J.-B., *Catal. Today*, 1997, vol. 36, no. 1, p. 25.
7. Koizumi, N., Jiang, X., Kugai, J., and Song, C., *Catal. Today*, 2012, vol. 194, no. 1, p. 16.
8. Saito, M., Fujitani, T., Takeuchi, M., and Watanabe, T., *Appl. Catal., A*, 1996, vol. 138, no. 2, p. 311.
9. Arena, F., Italiano, G., Barbera, K., Bordiga, S., Bonura, G., Spadaro, L., and Frusteri, F., *Appl.Catal., A*, 2008, vol. 350, no. 1, p. 16.
10. Graciani, J., Mudiyanselage, K., Xu, F., Baber, A.E., Evans, J., Senanayake, S.D., Stacchiola, D.J., Liu, P., Hrbek, J., Sanz, J.F., and Rodriguez, J.A., *Science*, 2014, vol. 345, no. 6196, p. 546.
11. Sahibzada, M., *Chem. Eng. Res. Des.*, 2000, vol. 78, no. 7, p. 943.
12. Bahruji, H., Bowker, M., Hutchings, G., Dimitratos, N., Wells, P., Gibson, E., Jones, W., Brookes, C., Morgan, D., and Lalev, G., *J. Catal.*, 2016, vol. 343, no. 1, p. 133.
13. Chiavassa, D.L., Barrandeguy, J., Bonivardi, A.L., and Baltanás, M.A., *Catal. Today*, 2008, vols. 133–135, no. 1, p. 780.
14. Liang, X.-L., Dong, X., Lin, G.-D., and Zhang, H.-B., *Appl. Catal., B*, 2009, vol. 88, no. 3, p. 315.
15. Fujitani, T., Saito, M., Kanai, Y., Watanabe, T., Nakamura, J., and Uchijima, T., *Appl.Catal., A*, 1995, vol. 125, no. 2, p. 199.
16. Shao, C., Fan, L., Fujimoto, K., and Iwasawa, Y., *Appl. Catal., A*, 1995, vol. 128, no. 1, p. 1.
17. Collins, S.E., Chiavassa, D.L., Bonivardi, A.L., and Baltanás, M.A., *Catal. Lett.*, 2005, vol. 103, no. 1, p. 83.
18. Zhang, L., Pan, L., Ni, C., Sun, T., Zhao, S., Wang, S., Wang, A., and Hu, Y., *Int. J. Hydrogen Energy*, 2013, vol. 38, no. 11, p. 4397.
19. Sonneveld, E.J. and Visser, J.W., *J. Appl. Crystallogr.*, 1975, vol. 8, no. 1, p. 1.
20. Ahouari, H., Soualah, A., Le Valant, A., Pinard, L., Magnoux, P., and Pouilloux, Y., *React. Kinet. Mech. Cat.*, 2013, vol. 110, no. 1, p. 131.
21. Zhang, B., Hui, S., Zhang, S., Ji, Y., Li, W., and Fang, D., *J. Nat. Gas Chem.*, 2012, vol. 21, no. 5, p. 563.
22. Huang, C., Chen, S., Fei, X., Liu, D., and Zhang, Y., *Catalysts*, 2015, vol. 5, no. 4, p. 1846.
23. Schuyten, S., Guerrero, S., Miller, J.T., Shibata, T., and Wolf, E.E., *Appl. Catal., A*, 2009, vol. 352, no. 1, p. 133.
24. Mierczynski, P., Ciesielski, R., Kedziora, A., Shtyka, O., and Maniecki, T.P., *Fibre Chem.*, 2016, vol. 48, no. 4, p. 271.
25. Jiang, X., Koizumi, N., Guo, X., and Song, C., *Appl. Catal., B*, 2015, vols. 170–171, no. 0, p. 173.
26. Jiang, X., Wang, X., Nie, X., Koizumi, N., Guo, X., and Song, C., *Catal. Today*, 2018, vol. 316, no. 1, p. 62.
27. Hu, B., Yin, Y., Liu, G., Chen, S., Hong, X., and Tsang, S.C.E., *J. Catal.*, 2018, vol. 359, no. 1, p. 17.
28. Melián-Cabrera, I., López Granados, M., and Fierro, J.L.G., *Catal. Lett.*, 2002, vol. 79, no. 1, p. 165.